AN AUGMENTED LAGRANGIAN METHOD FOR IMAGE RECONSTRUCTION WITH MULTIPLE FEATURES

H. Emre Güven, Alper Güngör

ASELSAN Inc., Ankara, Turkey
heguven@aselsan.com.tr
alpergungor@aselsan.com.tr

Müjdat Çetin

Faculty of Engineering and Natural Sciences,
Sabancı University, Istanbul, Turkey,
mcetin@sabanciuniv.edu

ABSTRACT

We present an Augmented Lagrangian Method (ALM) for solving image reconstruction problems with a cost function consisting of multiple regularization functions with a data fidelity constraint. The presented technique is used to solve inverse problems related to image reconstruction, including compressed sensing formulations. Our contributions include an improvement for reducing the number of computations required by an existing ALM method, an approach for obtaining the proximal mapping associated with p-norm based regularizers, and lastly a particular ALM for the constrained image reconstruction problem with a hybrid cost function including a weighted sum of the p-norm and the total variation of the image. We present examples from Synthetic Aperture Radar imaging and Computed Tomography.

Index Terms— Augmented Lagrangian Method, Image Reconstruction, Compressed Sensing, Alternating Direction Method of Multipliers, Sparsity

1. INTRODUCTION

We consider the problem of image reconstruction using constrained optimization techniques. Our technique enables successfully reconstructing images containing combination of sparse and piecewise-constant features. We model the scene as comprising of sparse and piecewise-constant features and solve the associated constrained optimization problem with a hybrid cost function, in a computationally efficient way thanks to Alternating Direction Method of Multipliers (ADMM), which is an Augmented Lagrangian Method (ALM).

ADMM techniques have been successfully applied to signal and image recovery problems [1, 2]. ADMM provides a divide-and-conquer approach by splitting unconstrained multi-objective convex optimization problems, augmenting the Lagrangian with a norm-squared error term, and using a nonlinear block Gauss-Seidel approach on the resultant terms in the optimization problem. The resulting algorithm exhibits guaranteed convergence under mild conditions [2].

In this paper, we propose a particular ADMM to solve a constrained optimization problem with the cost function given by a weighted sum of the p-norm and the total variation, for image reconstruction. In addition, we provide an approach for obtaining the proximal mapping associated with p-norms, together with an associated iterative reweighting algorithm within the ALM framework. We also present a computational improvement on a particular ADMM, called C-SALSA [2], when measurements are in a unitary transform domain, such as in Fourier space, as in synthetic aperture radar (SAR) and computed tomography (CT). We provide examples with a modified Shepp-Logan phantom simulation and TerraSAR data [3] to illustrate the benefits of the proposed method.

2. BACKGROUND

2.1. Observation Model

Many imaging problems, including SAR and CT, can be accurately modeled by linear operators in relating the vector containing image pixels to the data vector. Let the image vector be constructed by sequentially indexed pixel-values $\mathbf{x} \in \mathbf{C}^N$ and the observation kernel by the matrix $\mathbf{B} \in \mathbf{C}^{M \times N}$, which relates $\mathbf{x}$ to the measurement vector $\mathbf{y} \in \mathbf{C}^M$:

$$\mathbf{y} = \mathbf{B}\mathbf{x} + \mathbf{n}, \tag{1}$$

where $\mathbf{n} \in \mathbf{C}^M$ is the additive noise vector, typically from a normal distribution. In this paper, the data are assumed to be in the spatial Fourier domain (on a rectangular grid), therefore a two-dimensional Fourier transform operator relates the data vector to the unknown image. For CT, 1-D Fourier transforms of linear projections through Radon transformation yield the measurements in the Fourier space on radial lines. Similarly, spotlight-mode SAR phase history data lie on a polar grid in the spatial Fourier transform domain. Such data can be interpolated to a rectangular grid.

Algorithm 1: *C-SALSA* [2]

---

1. Set $k = 0$, choose $\mu > 0$, $\mathbf{z}_0^{(1)}, \mathbf{z}_0^{(2)}, \mathbf{d}_0^{(1)}, \mathbf{d}_0^{(2)}$
2. **repeat**
3. $\mathbf{r}_k = \mathbf{z}_k^{(1)} + \mathbf{d}_k^{(1)} + \mathbf{B}^H \left(\mathbf{z}_k^{(2)} + \mathbf{d}_k^{(2)} \right)$
4. $\mathbf{x}_{k+1} = \left(\mathbf{I} + \mathbf{B}^H \mathbf{B} \right)^{-1} \mathbf{r}_k$
5. $\mathbf{z}_{k+1}^{(1)} = \mathbf{\Psi}_{\phi/\mu} \left(\mathbf{x}_{k+1} - \mathbf{d}_k^{(1)} \right)$
6. $\mathbf{z}_{k+1}^{(2)} = \mathbf{\Psi}_{\iota_{E(\epsilon,\mathbf{I},\mathbf{y})}} \left(\mathbf{B}\mathbf{x}_{k+1} - \mathbf{d}_k^{(2)} \right)$
7. $\mathbf{d}_{k+1}^{(1)} = \mathbf{d}_k^{(1)} - \mathbf{x}_{k+1} + \mathbf{z}_{k+1}^{(1)}$
8. $\mathbf{d}_{k+1}^{(2)} = \mathbf{d}_k^{(2)} - \mathbf{B}\mathbf{x}_{k+1} + \mathbf{z}_{k+1}^{(2)}$
9. $k \leftarrow k + 1$
10. **until** some stopping criterion is satisfied.

2.2. Image reconstruction with priors

A constrained linear image reconstruction formulation involves solving the optimization problem

$$
\begin{aligned}
&\underset{\mathbf{x}}{\text{minimize}} && \phi(\mathbf{x}) \\
&\text{subject to} && \|\mathbf{B}\mathbf{x} - \mathbf{y}\|_2 \leq \epsilon
\end{aligned}
\tag{2}
$$

where $\phi(x)$ is the penalty function appropriately selected according to the reflectivity characteristics of the image, and the norm of the error in the data is prescribed to be smaller than a radius ϵ, that can be typically estimated from data. Depending on the selection of the penalty function $\phi(\mathbf{x})$, the characteristics of the reconstruction vary. In what follows, we consider the special cases with the p-norm $\|\mathbf{x}\|_p^p$ ($p \leq 1$) and the total variation of the image magnitude $TV(|\mathbf{x}|)$.

C-SALSA [2] (see Algorithm 1) is an ADMM technique for image recovery problems that benefits from the Augmented Lagrangian and variable splitting to efficiently solve problems of the form (2). The steps of C-SALSA include Moreau proximal mappings

$$
\mathbf{\Psi}_\phi(\mathbf{v}) = \text{prox}_{\phi(\cdot)}(\mathbf{v}) = \arg \min_x \ \phi(\mathbf{x}) + \frac{\mu}{2}\|\mathbf{x} - \mathbf{v}\|_2^2 \tag{3}
$$

such as those in steps 5 and 6 that are easy to implement, by soft thresholding for $\phi(\mathbf{x}) = \|\mathbf{x}\|_1$, Chambolle projections [7] for total variation $\phi(\mathbf{x}) = TV(\mathbf{x})$, and orthogonal projection $\mathbf{\Psi}_{\iota_{E(\epsilon,\mathbf{I},\mathbf{y})}}(\mathbf{s})$ onto the hypersphere for the data fidelity constraint, treated in an unconstrained form as an indicator function $\iota_{E(\epsilon,\mathbf{I},\mathbf{y})}$ of the set $E(\epsilon, \mathbf{I}, \mathbf{y}) = \left\{ \mathbf{x} \in \mathbf{C}^N : \|\mathbf{x} - \mathbf{y}\|_2 \leq \epsilon \right\}$. For further details, see [2].

3. PROPOSED APPROACH

In this section, we propose an algorithm based on ALMs, that involves (i) several improvements related to the number of transforms required in C-SALSA, (ii) proximal mappings associated with p-norms as well as an associated iterative reweighting algorithm, and (iii) a hybrid cost function

composed of a weighted sum of p-norm and total variation regularizers as well as an associated ADMM algorithm.

3.1. Improved C-SALSA for Unitary Transforms

C-SALSA requires several transformations in each iteration. For many imaging problems including SAR and CT, the data can be considered as gathered in the spatial frequency domain. As such, when the transformation matrix is unitary, we suggest that the number of transformations necessary for step 4 of C-SALSA can be further reduced. In such cases, the matrix $\mathbf{B}$ associated with the transformation can be decomposed as $\mathbf{B} = \mathbf{M}\mathbf{U}$, where $\mathbf{U}$ is unitary and $\mathbf{M}$ represents a binary masking operator defining which entries are observed as measurements [2], so that, by Woodbury's identity [2]:

$$
\left(\mathbf{I} + \mathbf{B}^H \mathbf{B} \right)^{-1} = \mathbf{I} - \frac{1}{2}\mathbf{U}^H \mathbf{M}^H \mathbf{M} \mathbf{U}. \tag{4}
$$

Following the definition of $\mathbf{r}_k$ in step 3 of C-SALSA:

$$
\mathbf{B}\mathbf{r}_k = \mathbf{B} \left(\mathbf{z}_k^{(1)} + \mathbf{d}_k^{(1)} \right) + \mathbf{B}\mathbf{B}^H \left(\mathbf{z}_k^{(2)} + \mathbf{d}_k^{(2)} \right). \tag{5}
$$

Together with $\mathbf{B}\mathbf{B}^H = \mathbf{I}$, it immediately follows that:

$$
\mathbf{B}\mathbf{r}_k = \mathbf{B} \left(\mathbf{z}_k^{(1)} + \mathbf{d}_k^{(1)} \right) + \left(\mathbf{z}_k^{(2)} + \mathbf{d}_k^{(2)} \right). \tag{6}
$$

Defining $\mathbf{q}_k = \mathbf{B} \left(\mathbf{z}_k^{(1)} + \mathbf{d}_k^{(1)} \right)$ results in:

$$
\mathbf{x}_{k+1} = \mathbf{z}_k^{(1)} + \mathbf{d}_k^{(1)} + \frac{1}{2}\mathbf{B}^H \left(\mathbf{z}_k^{(2)} + \mathbf{d}_k^{(2)} - \mathbf{q}_k \right) \tag{7}
$$

and

$$
\mathbf{B}\mathbf{x}_{k+1} = \mathbf{B} \left(\mathbf{z}_k^{(1)} + \mathbf{d}_k^{(1)} \right) + \frac{1}{2}\mathbf{B}\mathbf{B}^H \left(\mathbf{z}_k^{(2)} + \mathbf{d}_k^{(2)} - \mathbf{q}_k \right). \tag{8}
$$

Again, using $\mathbf{B}\mathbf{B}^H = \mathbf{I}$ we arrive at:

$$
\mathbf{B}\mathbf{x}_{k+1} = \frac{1}{2} \left(\mathbf{z}_k^{(2)} + \mathbf{d}_k^{(2)} + \mathbf{q}_k \right). \tag{9}
$$

Therefore, using Eq. (7), step 4 of C-SALSA can be solved using only one Fourier transform. Using Eq. (9), the vector $\mathbf{B}\mathbf{x}_{k+1}$ can be substituted in steps 6 and 8 of C-SALSA, without the need for a Fourier transform. The entire algorithm now requires only one 2-D FFT and one 2-D IFFT per iteration, instead of 4 FFTs suggested in [2] using Eq. (4).

3.2. Iteratively Reweighted Augmented Lagrangian Method (IRWALM)

Iterative reweighting has been applied in the context of solving non-convex optimization problems using known and simple proximal mapping functions [4].

Here, we provide a further refinement to C-SALSA, inspired by the effectiveness of p-norms used in the objective

function, as they have the potential to improve sparsity with $p < 1$. This general idea was first introduced in [5]. Here we present an approach for obtaining the proximal mapping associated with the p-norms. While the direct use of p-norms with $p < 1$ renders (2) non-convex, thus voiding any guarantees of global optimality; a locally-optimal solution is found nonetheless. A quasi-Newton method with a Hessian update scheme has been previously used successfully in a feature-enhanced SAR imaging context [6]. Here we apply the ADMM techniques for (2) with $\phi(\mathbf{x}) = \|\mathbf{x}\|_p^p$, with an approach we call Iteratively Reweighted Augmented Lagrangian Method (IRWALM), starting with the proximal mapping definition:

$$\text{prox}_{\|\cdot\|_p}(\mathbf{v}) = \arg\min_x \|\mathbf{x}\|_p^p + \frac{\mu}{2}\|\mathbf{x} - \mathbf{v}\|_2^2 \qquad (10)$$

To solve this equation, we take its derivative with respect to $\mathbf{x}$ and set it equal to 0 to obtain the reweighted mapping as:

$$\text{prox}_{\|\cdot\|_p}(\mathbf{v})[i] = \frac{1}{\mathbf{w}[i]} \text{soft}(\mathbf{w}[i] \times \mathbf{v}[i], p/\mu). \qquad (11)$$

where $\mathbf{v}[i]$ denotes the ith element of the vector $\mathbf{v}$, and $\mathbf{w}$ is the (re-)weighting vector in each iteration. Adding a small regularizer β to $\mathbf{w}$ as $\mathbf{w}[i] = (\mathbf{v}[i] + \beta)^{(1-p)}$ is helpful in practice to avoid numerically unstable divisions [4].

3.3. Hybrid IRWALM

Hybrid cost functions have been employed previously [6,8,9] with success in the context of sparsity-enhanced / compressive SAR imaging. In this paper, we propose an ADMM to solve the constrained optimization problem with the hybrid cost function:

$$\begin{aligned} \underset{\mathbf{z}^{(1)},\mathbf{z}^{(2)}}{\text{minimize}} \quad & \alpha_1\phi_1\left(\mathbf{z}^{(1)}\right) + \alpha_2\phi_2\left(\mathbf{z}^{(2)}\right) \\ \text{subject to} \quad & \|\mathbf{Bx} - \mathbf{y}\|_2 \le \epsilon, \; \mathbf{z}^{(1)} = \mathbf{z}^{(2)} \end{aligned} \qquad (12)$$

Letting $\mathbf{z} = \left[\mathbf{z}^{(1)}; \mathbf{z}^{(2)}; \mathbf{z}^{(3)}\right]$ and $\mathbf{G} = [\mathbf{I}; \mathbf{I}; \mathbf{B}]$, where the semicolon ';' denotes vertical stacking, we aim to solve:

$$\begin{aligned} \underset{\mathbf{x}}{\text{minimize}} \quad & f_1(\mathbf{x}) + f_2(\mathbf{z}) \\ \text{subject to} \quad & \mathbf{Px} + \mathbf{Qz} - \mathbf{m} = 0 \end{aligned} \qquad (13)$$

by setting $\mathbf{P} = \mathbf{G}, \mathbf{Q} = -\mathbf{I}, \mathbf{m} = 0, f_1(\mathbf{x}) = 0, f_2(\mathbf{z}) = \alpha_1\phi_1\left(\mathbf{z}^{(1)}\right) + \alpha_2\phi_2\left(\mathbf{z}^{(2)}\right) + \iota_{E(\epsilon,\mathbf{I},\mathbf{y})}\left(\mathbf{z}^{(3)}\right)$. This setting ensures that $\mathbf{Gx} = \mathbf{z}$, and consequently: $\mathbf{x} = \mathbf{z}^{(1)} = \mathbf{z}^{(2)}, \mathbf{Bx} = \mathbf{z}^{(3)}$. In the results section, we have chosen $\phi_1(\cdot) = \|\cdot\|_p^p$ and $\phi_2(\cdot) = TV(\cdot)$. We have worked with problems involving a unitary transform domain, namely, partial Fourier observations. To calculate the least squares, we use the Woodbury identity:

$$(2\mathbf{I} + \mathbf{B^H B})^{-1} = \frac{1}{2}(\mathbf{I} - \frac{1}{3}\mathbf{B^H B}). \qquad (14)$$

along with the formulation presented in Section 3.1, resulting in the computational steps provided in Algorithm 2.

Algorithm 2: *Hybrid IRWALM*


1. Set $k = 0$, $\beta_0 = 1$,
    choose $\mu > 0$, $\eta \in (0,1)$, $\mathbf{z}_0^{(1)}, \mathbf{z}_0^{(2)}, \mathbf{z}_0^{(3)}$,
        $\mathbf{d}_0^{(1)}, \mathbf{d}_0^{(2)}, \mathbf{d}_0^{(3)}, p, \alpha_1, \alpha_2$
2. **repeat**
3. $\mathbf{q}_k = \mathbf{B}(\mathbf{z}_k^{(1)} + \mathbf{d}_k^{(1)} + \mathbf{z}_k^{(2)} + \mathbf{d}_k^{(2)})$
4. $\mathbf{x}_{k+1} = \frac{1}{2}\left[\mathbf{z}_k^{(1)} + \mathbf{d}_k^{(1)} + \mathbf{z}_k^{(2)} + \mathbf{d}_k^{(2)} + \frac{1}{3}\mathbf{B}^H\left(2(\mathbf{z}_k^{(3)} + \mathbf{d}_k^{(3)}) - \mathbf{q}_k\right)\right]$
5. $\mathbf{w}_{k+1} = (\mathbf{x}_{k+1} - \mathbf{d}_{k+1}^{(1)} + \beta)^{(1-p)}$
6. $\mathbf{z}_{k+1}^{(1)} = \frac{1}{\mathbf{w}_{k+1}}\text{soft}(\mathbf{w}_{k+1} \times (\mathbf{x}_{k+1} - \mathbf{d}_k^{(1)}), \alpha_1 p/\mu)$
7. $\mathbf{z}_{k+1}^{(2)} = \Psi_{\frac{\alpha_2}{\mu}f_{22}}\left(\mathbf{x}_{k+1} - \mathbf{d}_k^{(2)}\right)$
8. $\mathbf{z}_{k+1}^{(3)} = \Psi_{\iota_{E(\epsilon,\mathbf{I},\mathbf{y})}}\left(\frac{1}{3}(\mathbf{q}_k + \mathbf{z}_k^{(3)} + \mathbf{d}_k^{(3)}) - \mathbf{d}_k^{(3)}\right)$
9. $\mathbf{d}_{k+1}^{(1)} = \mathbf{d}_k^{(1)} - \mathbf{x}_{k+1} + \mathbf{z}_{k+1}^{(1)}$
10. $\mathbf{d}_{k+1}^{(2)} = \mathbf{d}_k^{(2)} - \mathbf{x}_{k+1} + \mathbf{z}_{k+1}^{(2)}$
11. $\mathbf{d}_{k+1}^{(3)} = \mathbf{d}_k^{(3)} - \frac{1}{3}\left(\mathbf{q}_k + \mathbf{z}_k^{(3)} + \mathbf{d}_k^{(3)}\right) + \mathbf{z}_{k+1}^{(3)}$
12. $k \leftarrow k + 1$
13. **until** some stopping criterion is satisfied.

---

4. RESULTS

The algorithm is implemented in MATLAB, where the Chambolle projections are called from a mex function. The experiments were conducted on a workstation with Intel Core i5-3470 CPU and 8 GB of RAM. All values are initialized to zero except for $\mathbf{z}_0^{(3)} = \mathbf{y}$. The inner iterations for Chambolle projections [7] are repeated 5 times per outer iteration. We have chosen μ as 300, and stopping criterion as $\|\mathbf{z}_{k+1}^{(1)} - \mathbf{z}_k^{(1)}\|_2^2 < 10^{-3}$ and $\|\mathbf{z}_{k+1}^{(2)} - \mathbf{z}_k^{(2)}\|_2^2 < 10^{-3}$ or 200 iterations maximum.

In order to study the effect of the hybrid cost function, we consider an image from TerraSAR [3]. A relative weighting of $\alpha_1 = 0.8$ for $p = 0.8$-norm and $\alpha_2 = 0.2$ for total variation of the image magnitude is chosen. Figure 1 shows the reference image, the binary spectral mask, where available data samples relative to those used for the reference image are 39%, as well as conventional, p-norm, min-TV, and hybrid reconstructions. The contrast across piecewise-constant features are improved by using the hybrid-cost significantly relative to the p-norm reconstruction, while better maintaining super-resolution features compared to the min-TV solution. Table 1 shows the imaging times of our proposed IRWALM approach compared to Feature Enhanced Reconstruction Method (FERM) [6], which involves another algorithm for solving the sparse optimization problem, for the TerraSAR example. Average computation times and cost function values over 20 runs are given, where $p = 0.8$ $\mu = 300$ $\alpha_1 = 0.8, \alpha_{TV} = 0.2$. The proposed hybrid IRWALM is computationally more efficient, and bears a potential for parallel implementation.

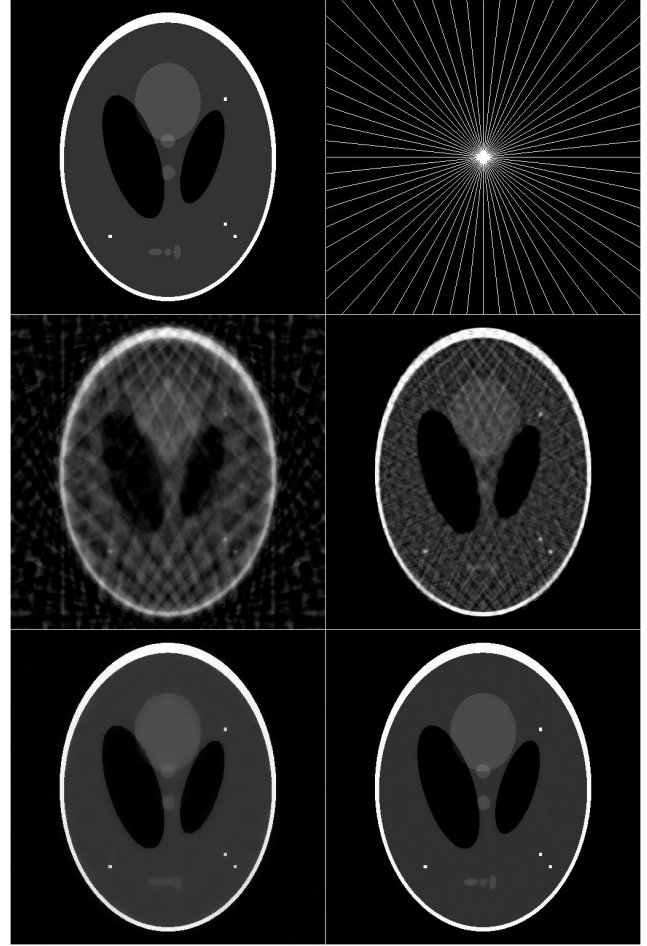Next, we provide an example from Computed Tomogra-
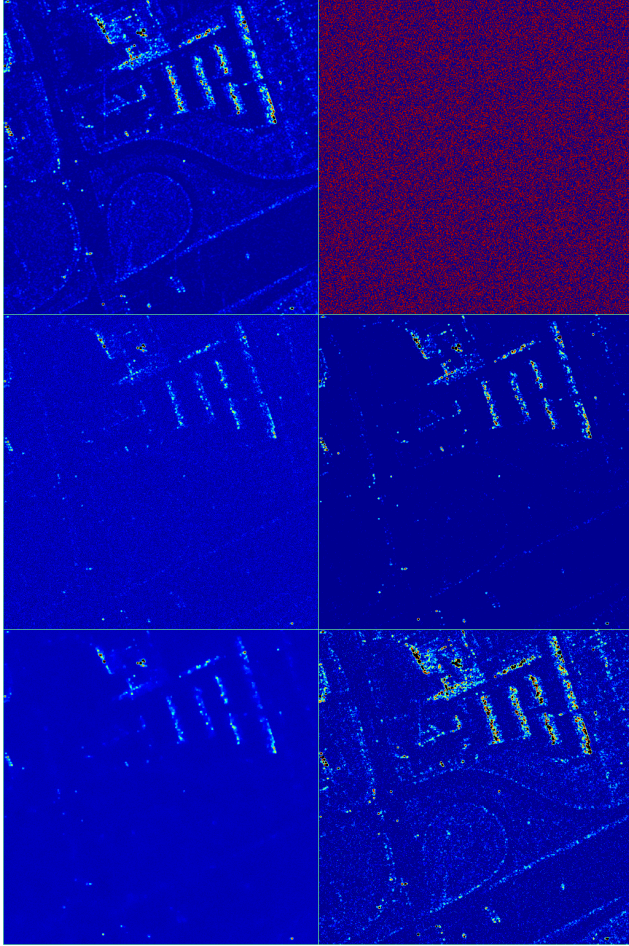
Fig. 1. Reference TerraSAR image (upper-left); binary mask in Fourier space (upper-right); and reconstructions: conventional (middle-left), 0.8-norm (middle-right), min-TV (lower-left), hybrid-cost (lower-right)

Fig. 2. Original phantom (upper-left); binary mask in Fourier space (upper-right); and reconstructions: conventional (middle-left), 1-norm (middle-right), min-TV (lower-left), hybrid-cost (lower-right)

phy where the data in the spatial frequency domain are obtained in pixels on radial lines [10]. The ratio of available samples in the spatial frequency domain relative to the full number of samples is 6%. Fig. 2 shows the original image (Shepp-Logan phantom with added sparse components), the spectral lines where data are available, conventional reconstruction with zero-filling, and reconstructions with 1-norm, min-TV, and hybrid cost functions. Note that the reconstruction with only total variation as the cost function does not perform as well as the reconstructed images with the hybrid cost function, especially for circular components in the image, and the 1-norm reconstruction is not as successful either.

5. DISCUSSION

We have proposed an efficient method based on Augmented Lagrangian Methods for constrained imaging problems with hybrid cost functions. The suggested improvements over the C-SALSA technique include the reduction of the number of FFTs in each iteration, an iterative reweighting enabling the use of p-norms in the cost function, and an ADMM for hybrid cost functions. Results for SAR and CT imaging examples demonstrate the desirable performance of our approach in terms of image reconstruction quality, as well as computational improvements it provides over another sparsity-based algorithm.

Mask	t_{FERM}	t_{IRWALM}	$\frac{\varepsilon_{\text{IRWALM}}}{\varepsilon_{\text{FERM}}}$	$\frac{cost(x_{\text{IRWALM}})}{cost(x_{\text{FERM}})}$
Rand (39%)	11.87 s	2.78 s	1.00	0.96
Rand (22%)	15.33 s	2.82 s	1.00	0.96
Rand (12%)	23.01 s	3.55 s	1.00	0.90
Rand (6%)	30.20 s	3.35 s	0.99	0.98

Table 1. Computation times, error- and cost-ratios for FERM and Hybrid IRWALM

6. REFERENCES

[1] S. Boyd, N. Parikh, E. Chu, B. Peleato, and J. Eckstein, "Distributed optimization and statistical learning via the alternating direction method of multipliers," *Foundations and Trends in Machine Learning*, vol. 3, no. 1, pp. 1–122, 2011.

[2] M. Afonso, J. M. Bioucas-Dias, and M. A. T. Figueiredo, "An Augmented Lagrangian approach to the constrained optimization formulation of imaging inverse problems," *IEEE Trans. Image Processing*, vol. 20, pp. 681–695, Mar. 2011.

[3] Astrium TerraSAR-X sample imagery: http://www.astrium-geo.com/en/23-sample-imagery

[4] R. Chartrand and W. Yin, "Iteratively reweighted algorithms for compressive sensing," in *Proc. IEEE International Conference on Acoustics, Speech, and Signal Processing*, 2008.

[5] H. E. Guven and M. Cetin, "An Augmented Lagrangian method for sparse SAR imaging," in *10th European Conference on Synthetic Aperture Radar (EUSAR 2014)*. EU, 2014.

[6] M. Cetin and W. C. Karl, "Feature-enhanced Synthetic Aperture Radar image formation based on nonquadratic regularization," *IEEE Trans. Image Processing*, vol. 10, pp. 623–631, Apr. 2001.

[7] A. Chambolle, "An algorithm for total variation minimization and applications," *J. Math. Imag. Vis.*, vol. 20, pp. 89–97, 2004.

[8] V. M. Patel, G. R. Easley, D. M. Healy, Jr. and R. Chellappa, "Compressed Synthetic Aperture Radar," *IEEE Journal of Selected Topics in Signal Processing: Special Issue on Compressive Sensing*, vol. 4, no. 2, pp. 244–254, Apr. 2010.

[9] S. Samadi, M. Cetin, and M. A. M. Masnadi-Shirazi, "Multiple Feature-Enhanced SAR Imaging using Sparsity in Combined Dictionaries," *IEEE Geoscience and Remote Sensing Letters*, vol. 10, no. 4, pp. 821–825, Jul. 2013.

[10] E. J. Candès, J. Romberg, and T. Tao, "Robust uncertainty principles: Exact signal reconstruction from highly incomplete frequency information," *IEEE Transactions on Information Theory*, vol. 52, no. 2, pp. 489–509, Feb. 2006.